www.sciencemag.org/content/351/6272/488/suppl/DC1

Supplementary Materials for

Periodic slow slip triggers megathrust zone earthquakes in northeastern Japan

Naoki Uchida,* Takeshi Iinuma, Robert M. Nadeau, Roland Bürgmann, Ryota Hino

*Corresponding author. E-mail: naoki.uchida.b6@tohoku.ac.jp

Published 29 January 2016, *Science* **351**, 488 (2016)
DOI: 10.1126/science.aad3108

This PDF file includes:

Materials and Methods
Figs. S1 to S14
Tables S2 to S4
References (*31*–*42*)

Other Supplementary Materials for this manuscript include the following:
(available at www.sciencemag.org/content/351/6272/488/suppl/DC1

Table S1

Methods

Slip rate estimation from repeating earthquakes

We used Uchida and Matsuzawa (2013)'s catalogue (*10*) in which repeating earthquakes are selected based on waveform similarity. The waveform data used here are vertical component data from the microearthquake observation network of Hokkaido University, Hirosaki University, Tohoku University and the University of Tokyo (Fig. 2A). Most of the seismometers are of 1 Hz velocity type with sampling frequency of 100 Hz and for the period from 1984 to 2011 (36.5º – 41.5ºN) and 1993 to 2011 (to the south of 36.5º and to the north of 41.5ºN). The catalogue contains earthquakes larger than M2.5 before the Tohoku-oki earthquake and larger than M4.0 after the earthquake. This difference is because the earthquake catalogue is not complete for events smaller than M4.0 after the Tohoku-oki earthquake. Coherence of earthquake pairs for fixed time windows of 40 s from the P wave arrival that always include S phase arrivals, and these were evaluated to select repeating earthquakes. For earthquakes from M2.5 to M4.0, the similarity threshold is 0.95 for averaged coherencies in the 1 - 8 Hz band. For earthquakes larger than M4.0, we choose the frequency band around the corner frequency of the smaller event in the pair (1/2 to 2 times the corner frequency) and the coherence threshold is 0.8. The thresholds were determined based on the frequency distribution of coherence and the hypocenter locations of earthquakes determined precisely by waveform-based differential time data for the off-Kamaishi repeaters (*31*). The focal mechanisms of the repeating earthquakes are of low-angle thrust type (*10*), suggesting that they are occurring on the plate boundary.

After the selection of repeating earthquakes, the slip for each small repeating earthquake was estimated based on the following relationship between the seismic moment (Mo; dyne·cm) and fault slip (d; cm) (*32*)

$$\log(d) = -2.36 + 0.17\log(M_0) \tag{1}$$

This empirical relationship was obtained from shallow repeating earthquake data in California. The seismic moment was estimated from the following relationship between the moment and magnitude (M) (*33*).

$$\log(M_0) = 1.5M + 16.1. \tag{2}$$

The magnitude used here is determined by the Japan Meteorological Agency.

The periodicity or recurrence intervals of individual repeating earthquake sequences is sometimes studied to understand the nature of recurrent earthquakes (e.g., 34, 35). The repeating earthquakes are thought to be recurring in relatively regular intervals if the aseismic slip rate in the surrounding area is constant. In this study, however, we focus on time-varying aseismic slip that can be estimated from many repeating earthquake sequences. We estimate slip rates in each time period and area, estimated by dividing the cumulative slip by time and averaging all the repeating sequences in an area. The averaged slip rate expresses aseismic slip rate in the area and is not directly related to the recurrence intervals of each sequence if many repeating earthquakes are used for the averaging. In this study we used more than 10 sequences in the averaging process.

We estimated 0.5-year averaged slip rate stepping in 0.1-year intervals from all repeater sequences in each area. The choice of the averaging time window length (0.5 year) affects the estimated slip rate but does not strongly impact the inferred periodicity

(Fig. S14). The estimated slip rate is plotted at the center of each window. The use of different relationships between the magnitude and slip (eqs. 1 and 2) will yield a slightly different slip rate. Igarashi et al. (2003) (36) confirmed that the slip estimate from Nadeau and Johnson's relationship applied to the time intervals between repeating earthquakes close to the coast of northeastern Japan is consistent with the slip estimated from the long-term relative plate motion. Chen et al., (2007) (34) show that the relationship is applicable to Parkfield, NE Japan and eastern Taiwan. Mavrommatis et al (2015) (37) suggest similarly good fits to data for Beeler et al. (2001) (38)'s model and Nadeau and Johnson's model (32). Therefore, we consider Nadeau and Johnson's relationship fully appropriate for the slip estimate and the use of different relationships would not affect the inferred periodicity of slip-rate variation.

Figure 1 schematically shows the analyses steps described above. Suppose there are only three repeater sequences in area A (Fig. 1B). Note that the actual data has at least 10 sequences for the estimation of the spatial distribution of slip rate periodicity (Fig., 2, Fig. 4). Repeater sequence 1 has three earthquakes (EQ 1 – 3) whose waveforms are shown in Fig. 1C. Figure 1D illustrates the repeater activity showing the occurrence time of each earthquake by circles. This corresponds to the top figures of for real data shown in Figs. 2 B and C and Fig. S3. By calculating the slip of each earthquake with equation (1), we can obtain cumulative slip for each repeater sequence (Fig. 1E). By averaging the cumulative slip for the three repeater sequences, we obtain averaged cumulative slip estimates in area A (Fig. 1F). We consider this to reflect the temporal evolution of aseismic fault creep in area A. The temporal change of slip rate in area A is obtained from the gradient of the cumulative slip by using a 0.5-year sliding time window (Fig. 1G). This corresponds to the bottom figures for the real data shown in Figs. 2 B and C and Figs. S3.

The spectrum analyses and fitting of sinusoid to the observations are performed based on the final slip-rate time series. We consider only periods ranging from 1 – 9 years, constrained by the observation time period (28 years) and the smoothing window (0.5 year). In the sinusoid fitting, we seek optimum period yielding the largest cross-correlation-coefficient with changing period about the peak period of the slip-rate spectrum shown in Figs. S6A and S6B. We define the phase of the sinusoidal function so that it is positive when the function value exceeds the average. Note that the periods estimated from the two methods are slightly different but the differences are insignificant (Fig. S3 and Table S2).

Estimation of temporal change of the interplate coupling from GPS data

One of the major factors that determine horizontal ground velocity of the forearc area is interplate coupling (*20, 39*). We estimated the temporal change in the interplate coupling along the subducting plate interface in NE Japan based on the spatial gradients of the surface displacement rates estimated from on-land GPS data (Fig. 1A). We assume most of the interplate locking occurs in the offshore region according to previous studies (*39*). If the interplate locking is strong, the surface landward deformation becomes larger towards the trench (Fig. S12A). This spatial difference in velocity can be expressed as a velocity gradient (Fig. S12C). If the locking ratio changes, the gradient changes (Figs. S12B and 12D). To estimate the temporal change of velocity gradient, we used daily site coordinate time series of GEONET (F3 solutions) that have been provided by the Geospatial Information Authority of Japan.

First, we extract displacement rates at each GPS station from the site coordinate time series by fitting a mathematical function that consists of long-term linear trend, annual and biannual trigonometric curve, and steps due to earthquakes and antenna replacements. We assign 5 year time windows ending every Monday from 24 March 1997 to 22 July 2013. For the long-term linear trends, we divides the 5-year window into five successive 1-year windows that the value at the junction of the 1-year time windows are continuous (i.e. polygonal line). We regarded the linear trend estimated for the latest 1-year time window as the average velocity at the time window. Note that first 4-year time windows are used for the estimation of annual and biannual trigonometric curve, and steps but not used for the final 1-year average velocity. Applying this time series fitting procedure for coordinate time series of all GPS stations, we can obtain weekly surface velocity field.

The gradient of the surface velocities is calculated for each 30-km-wide profile region configured along the plate convergence direction (Fig. S2A). Horizontal velocities are projected into this direction. Spatial gradients of the surface horizontal velocities are estimated with linear regression for velocities of GPS stations inside the region excluding the velocities that are estimated from the time series shorter than 1 year. In Figs. S12E-H, we show examples of GPS velocities and gradients for two periods. The two periods show contrasting velocity gradients that can be interpret as strongly (Figs. S12E and G) and weakly (Figs. 12F and H) locked (coupled) periods in the offshore plate boundary. Positive horizontal velocity gradients indicate that the closer to the Japan trench a particular point is, the larger its eastward (N105ºE) velocity is.

We performed synthetic tests using forward dislocation models for assumed interplate coupling distributions, and found that 1) a large negative horizontal velocity gradient corresponds to strong interplate coupling at shallow to intermediate depth (less than about 50 km in depth), and 2) the negative velocity gradient goes towards zero when the plate interface beneath the land is not coupled. Therefore, we can capture the temporal change in the interplate coupling on the plate interface offshore the Northeast Japan by monitoring the temporal change in the horizontal velocity gradient. The temporal change of the velocity gradient and its spectrum is shown in Fig. S13. The inferred periodicities shown by colored circles in Fig. 4 are the peak periods shown by green circles in Fig. S13.

The overall decreasing trend of GPS-gradient throughout the observation period in area D and near-shore Sanriku is probably due to the locking recovery (deceleration of postseismic slip) after the 1994 Sanriku-oki earthquake (M7.6, Fig. 2A) that occurred close to these area (*40*).

<u>Estimation of slow-slip period and its uncertainty</u>

The dominant period of slow slip is estimated from the peak of the spectrum of slip rate curve (Fig. 3B). The uncertainty of the peak is estimated by bootstrapping the repeater data to estimate slip rate curves as follows. Note that we have 10 or more repeater groups for the estimate of slip rates. We randomly select repeaters in each area allowing duplication and estimate peak period within 2 years of the original dominant period. The 2-year band is used to estimate the uncertainty of the main spectrum peak without the effect of secondary peaks. The random resampling is executed 300 times to obtain the standard deviation of the peak period. We regard the standard deviation as the uncertainty of the dominant period.

Estimation of the earthquake number ratio in the positive and negative phase of sinusoidal curve fitted to the slip-rate changes

The earthquake number ratio of earthquakes in positive and negative period of the sinusoids fitted to the slip rate curve was simply estimated by counting earthquake number within the positive and negative phase. In addition to the original data, we counted the ratio for data from Reasenberg [1985]'(*41*)s declustering method (program cluster2000x) that identifies aftershocks based on a physical two-parameter model of the earthquake interaction process. We also check the stability by using a range of declustering parameters (Tables S3 and S4).

Supplementary Text

Supplementary figures 1 to 14

Supplementary figures referred in the Methods and main text are shown below.

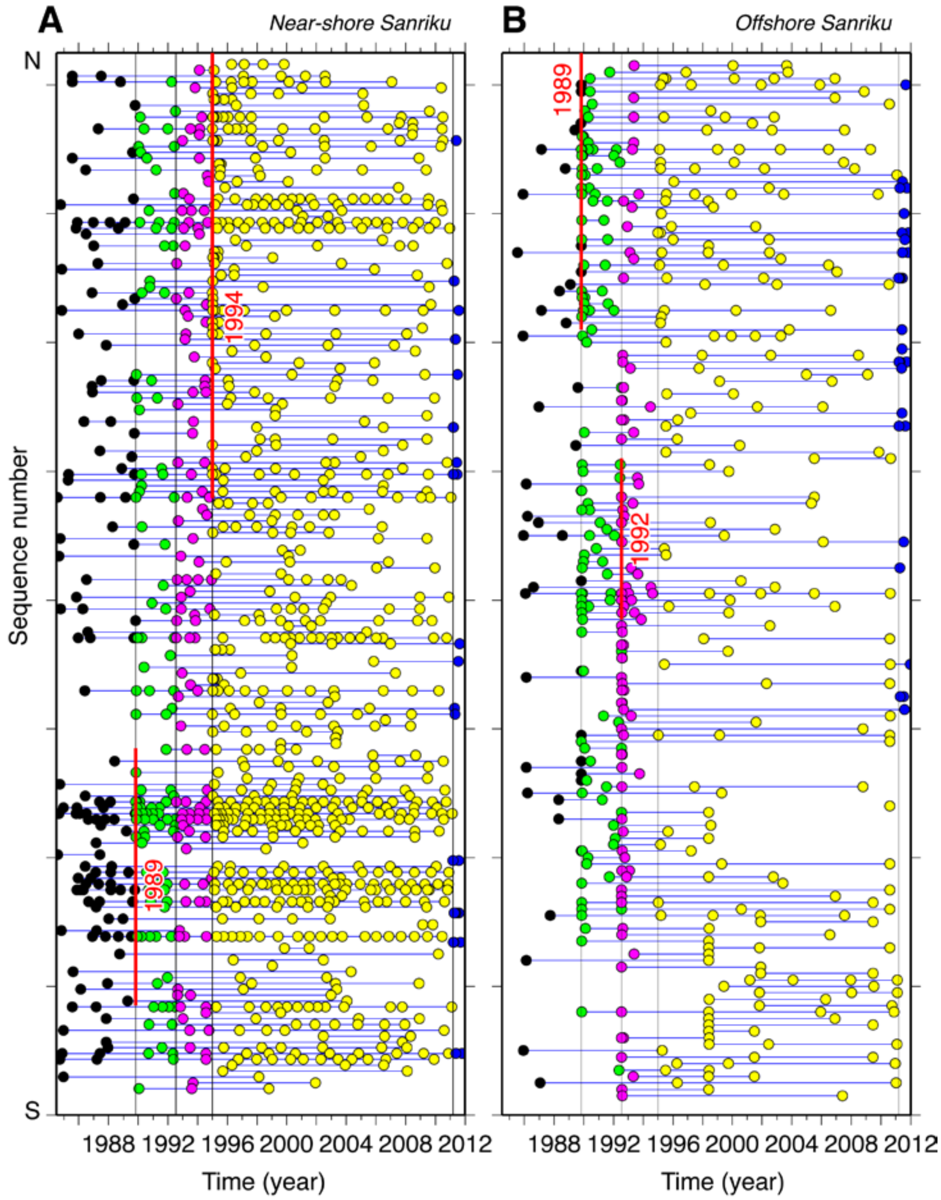

Fig. S1.

Temporal distribution of small repeating earthquakes for near-shore Sanriku (A) and offshore Sanriku (B) areas. The areas are shown in Fig. 2A. Circles show the occurrence time of each earthquake and horizontal lines connect the earthquakes that belong to the same sequence. Sequences are aligned from north to south. Vertical lines denote the occurrence times of the 1989 (M7.2), 1992 (M6.9) and 1994 (M7.6) Sanriku-oki earthquakes and the 2011 Tohoku-oki earthquake (M9.0) (See Fig. 2 for the epicenters). Red vertical lines show the approximate rupture extent of these events from Yamanaka and Kikuchi, 2004 (*12*). The circles are color-coded depending on the period between these earthquakes. Note that some of the repeating earthquakes occurred just before the four major earthquakes

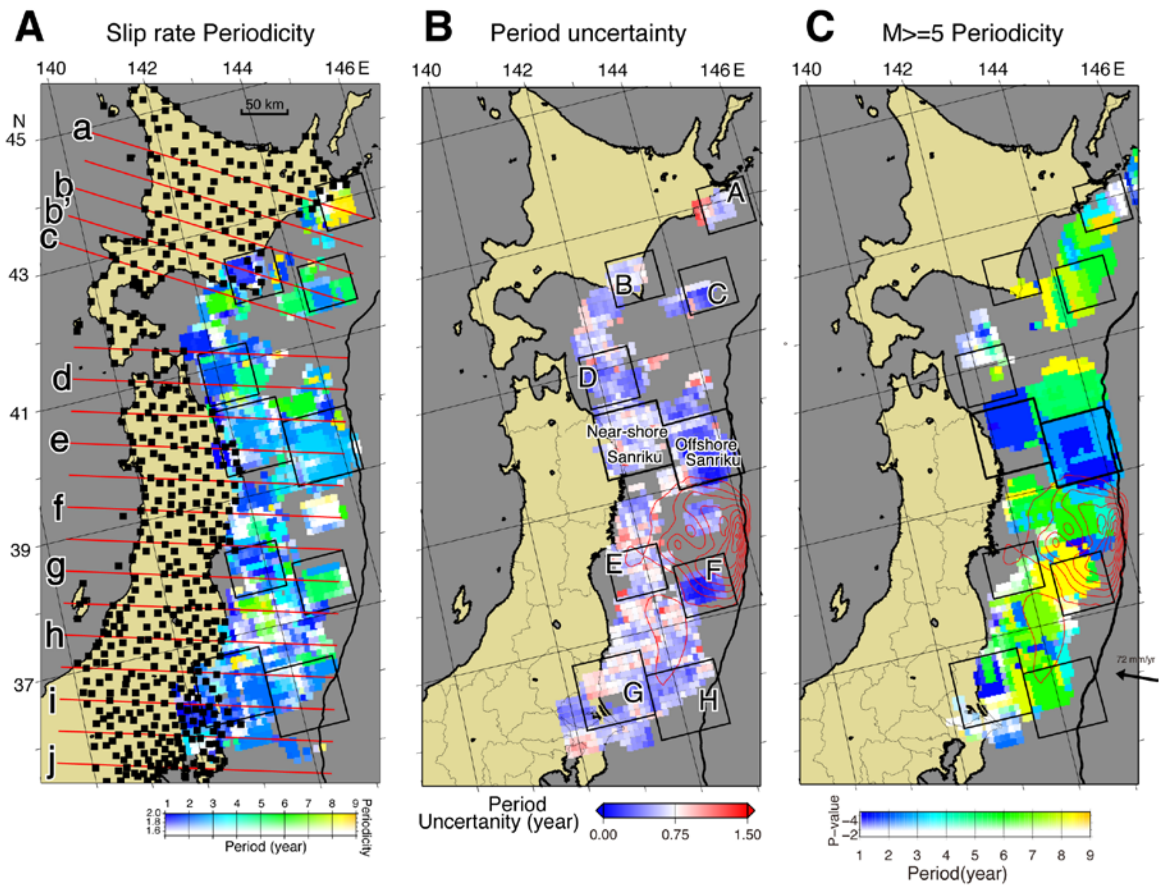

Fig. S2

(A) Map showing GPS stations (squares), profile lines of the GPS data analyses (red lines) and analyses area of the repeating earthquakes (black rectangles). Colors in the offshore area are the same as those on Fig. 4 (Spatial distribution of periodicity (color intensity) and dominant period (color) of interplate slip velocity estimated from small repeating earthquakes). (B) Uncertainty of periodicity that was estimated for repeater-derived slip-rate. (C) The distribution of dominant period (peak p-value) of M ≥ 5 earthquakes for the period from 1984 to March 11, 2011 (before the Tohoku-oki earthquake). The spatial window size is 0.8 degree (latitude) by 2.0 degree (longitude). The estimation was performed for areas 20 or larger M ≥ 5 earthquake exist.

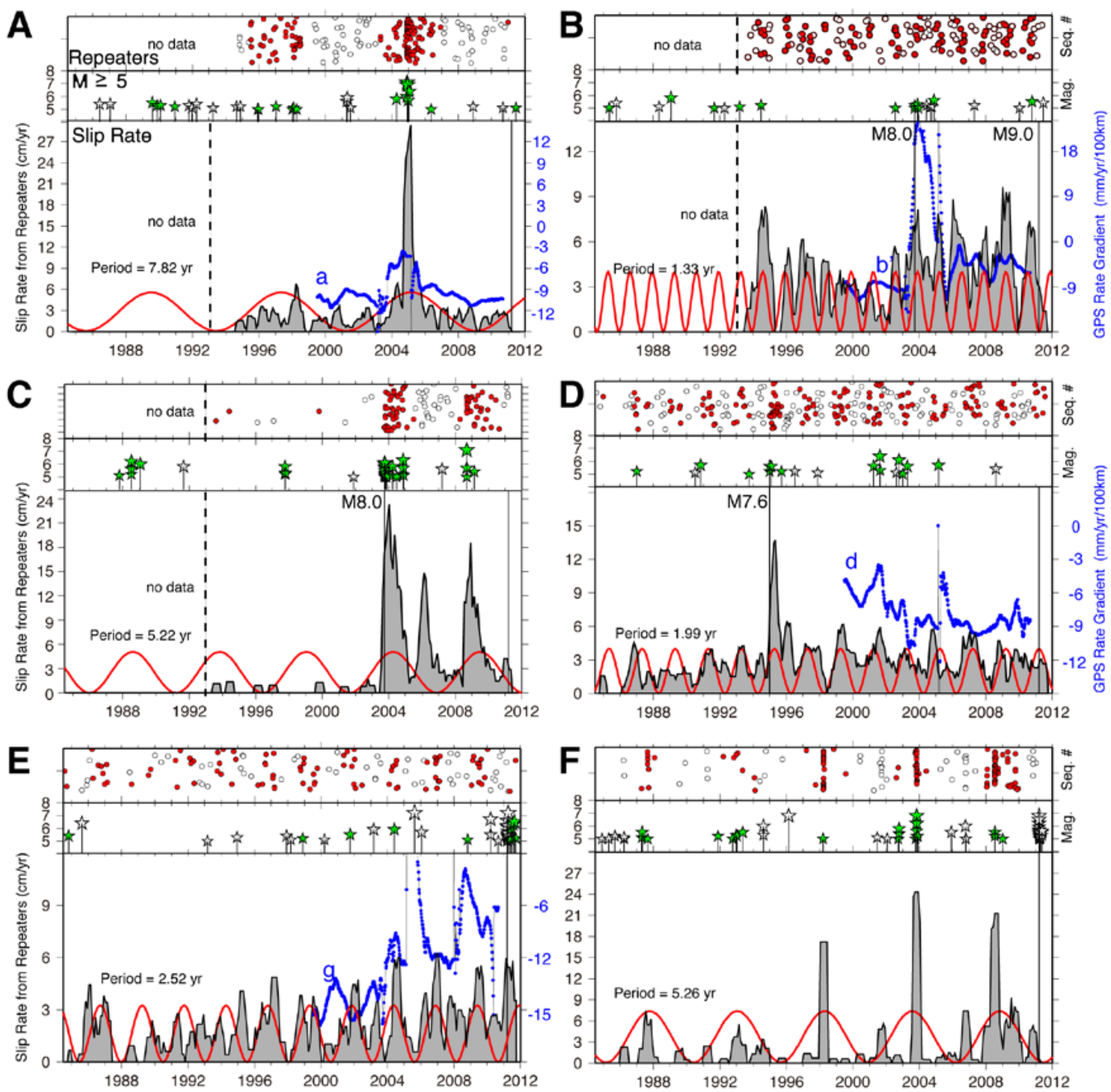

Fig. S3

Temporal distribution of small repeating earthquakes (top), magnitude-time plot of M ≥ 5 earthquakes (middle) and temporal change of slip rate inferred from repeating earthquakes (bottom) for areas A-H that are shown in Fig. S2 and offshore (I) and near-shore Sanriku (J) areas. Vertical lines show the times of the 1994 Sanriku-oki (M7.6), 2003 Tokachi-oki (M8.0) and the 2011 Tohoku-oki (M9.0) earthquakes. Red curves are sinusoidal functions fit to the slip rate changes. The best-fit periods are shown in each panel. The colored and white symbols for repeating earthquakes and M ≥ 5 earthquakes show events during times of positive and negative amplitude of the sinusoid, respectively. Blue lines show temporal change of horizontal land velocity gradient estimated from on-land GPS stations for near-shore areas. Note that the GPS velocity gradient scales are shown in blue on the right and analysis profiles are shown in Fig. S2A).

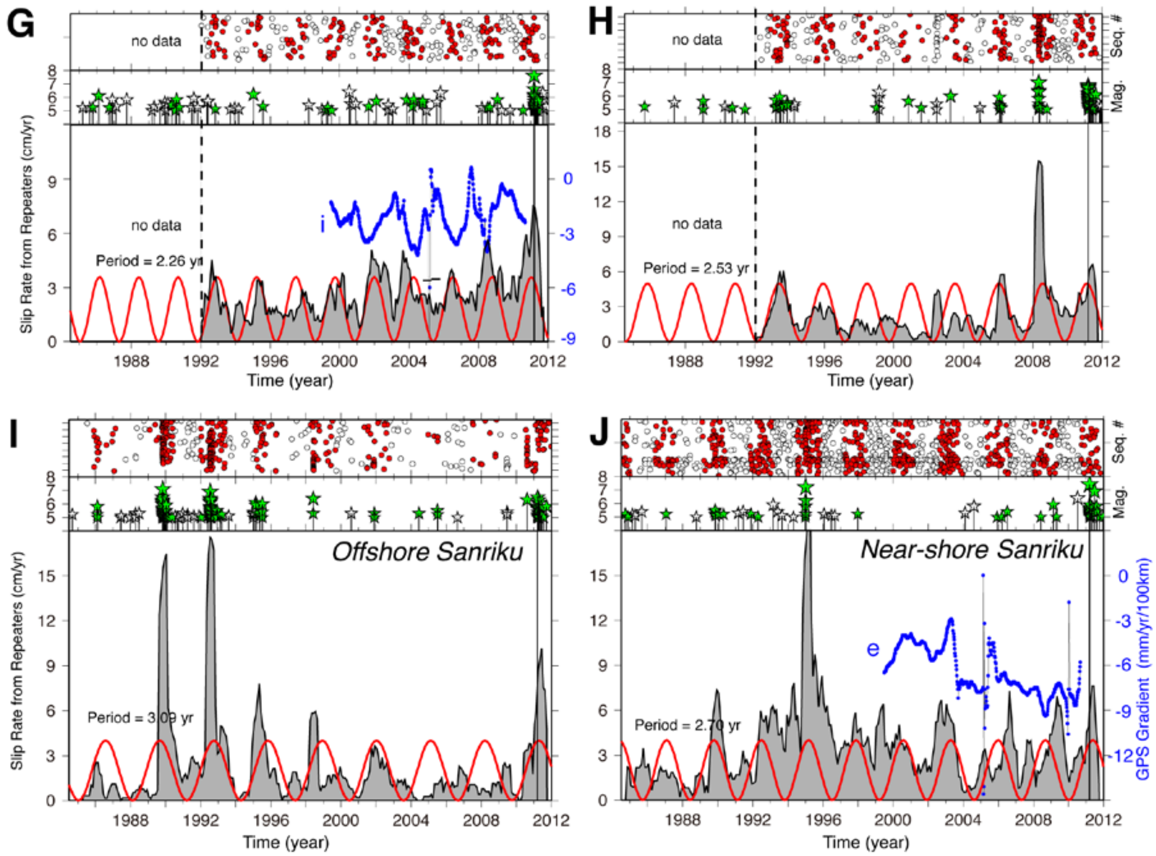

Fig. S3 (continue)

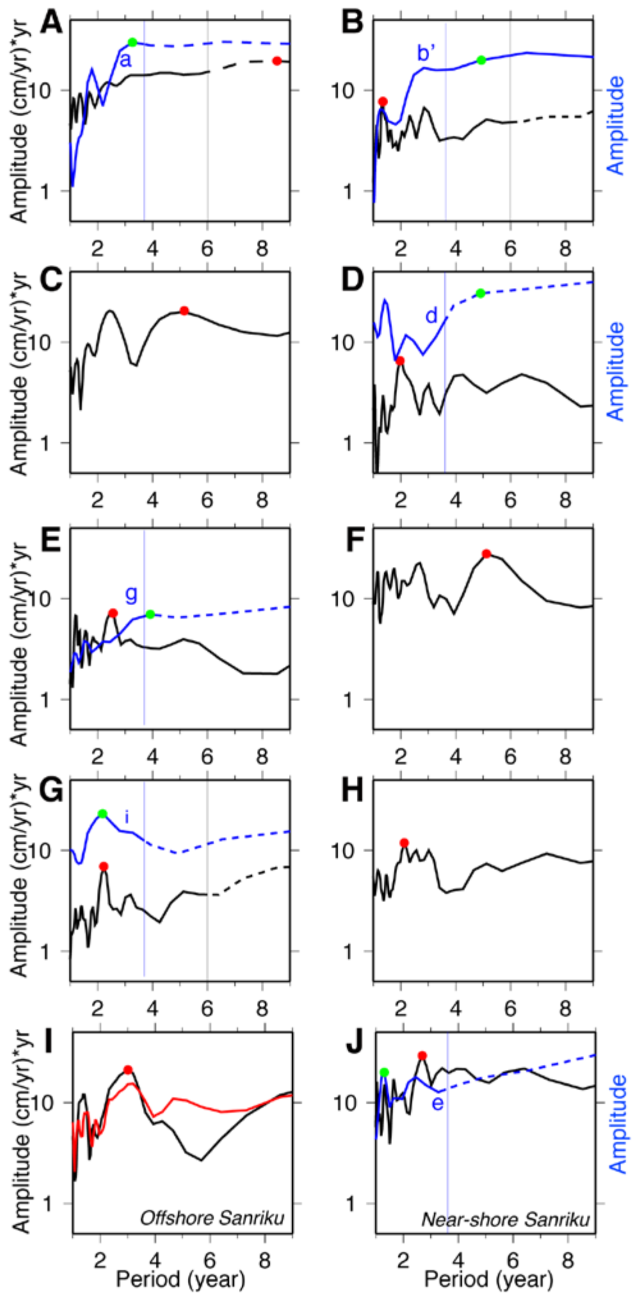

Fig. S4

Amplitude spectra of slip-rate time series for areas A-H shown in Fig. S2 and offshore Sanriku, near-shore Sanriku areas shown in Fig. 2A. The original slip-rate time series are shown in Fig. S3 and Figs. 2B, C. Red line in (I) shows spectrum for a limited period from 1992 to 2011 to exclude two large earthquakes in 1989 and 1992. Also shown with a blue line is the amplitude spectra of GPS gradient shown in Fig S3. Red and green dots show the peak of the amplitude spectrum in each panel. Dashed lines show spectra for the periods that are not constrained by 3 or more cycles. Note that the GPS data span 11 years, while the repeater data period is 19 or 28 years long.

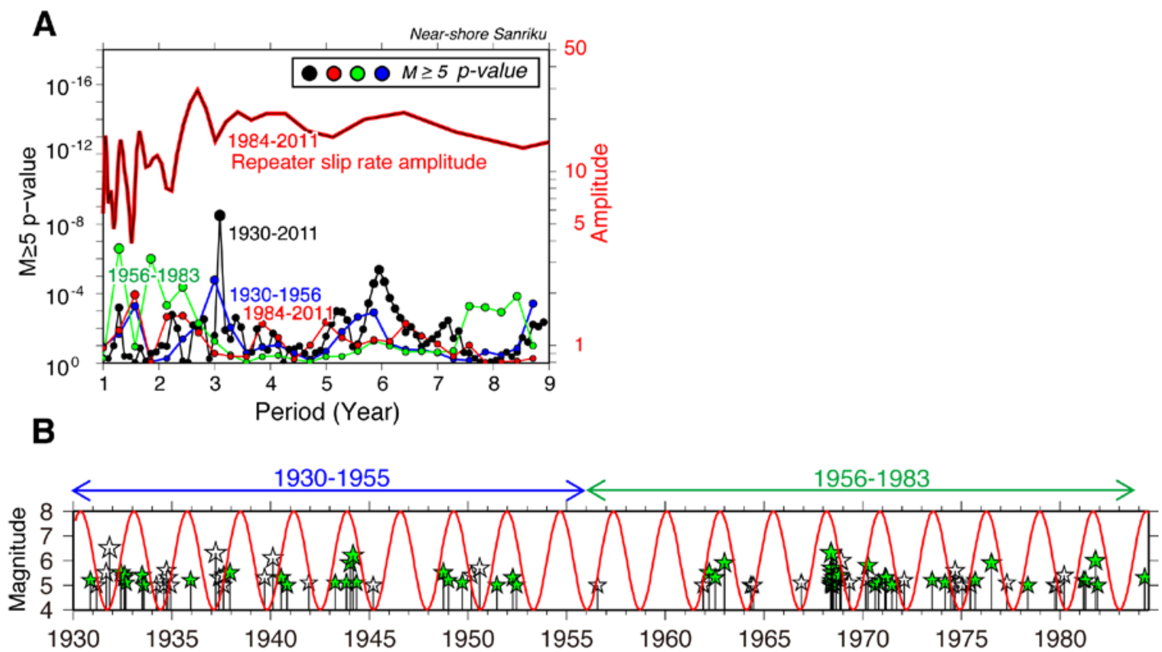

Fig. S5

(A) Schuster spectra (*19*) for M ≥ 5 earthquakes in the near-shore Sanriku area for four time periods shown in the figure (black, red, green, and blue circles). Amplitude spectrum of the slip rate from the repeating earthquake data is also shown by red line. (B) Magnitude vs. time plot of M ≥ 5 earthquakes in the near-shore Sanriku area for the period before the repeater analysis period (from 1930 to 1983). Red curve is the same sinusoidal function as in Fig. 2C that is extrapolated back in time from the original fitting range. Green and blue bidirectional arrows show the time periods used in Fig. S5A.

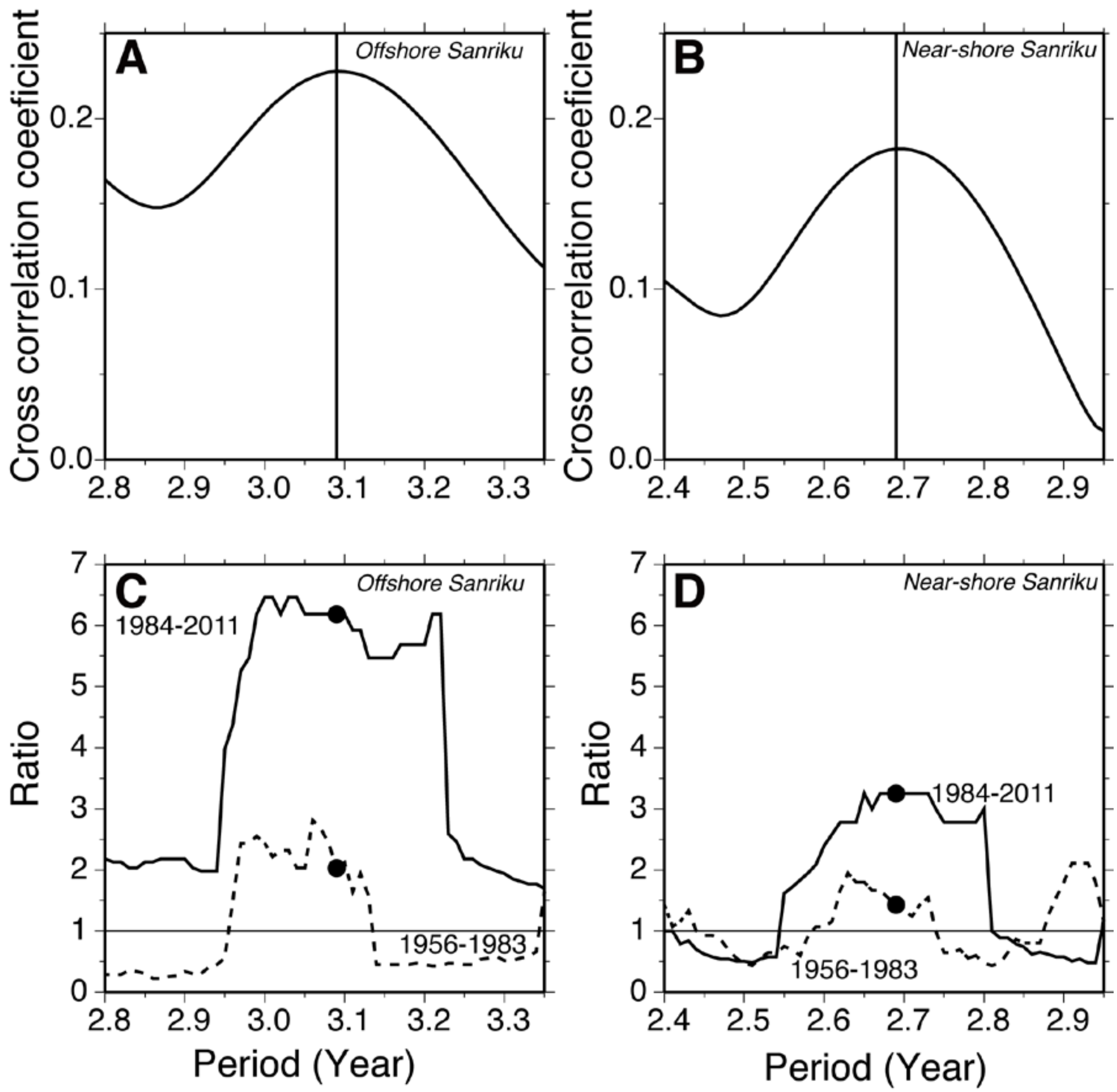

Fig. S6

Periodic slip rate and occurrence of M ≥ 5 earthquakes. (A and B) Cross-correlation-coefficient between the sinusoidal function and the slip-rate time series for a range of periods around that estimated from the spectral analyses for offshore Sanriku (A) and near-shore Sanriku (B) areas. (C and D) The ratio of M ≥ 5 earthquake number in positive phase of the sinusoidal curve fitted to the slip velocity to the number in negative phase for a range of periods. (C) and (D) are for the offshore and near-shore Sanriku, respectively. Black and dashed curves are for the period from 1984 to 2011 and 1956 to 1983, respectively. Black dots show the ratio for the period with the largest cross-correlation-coefficient.

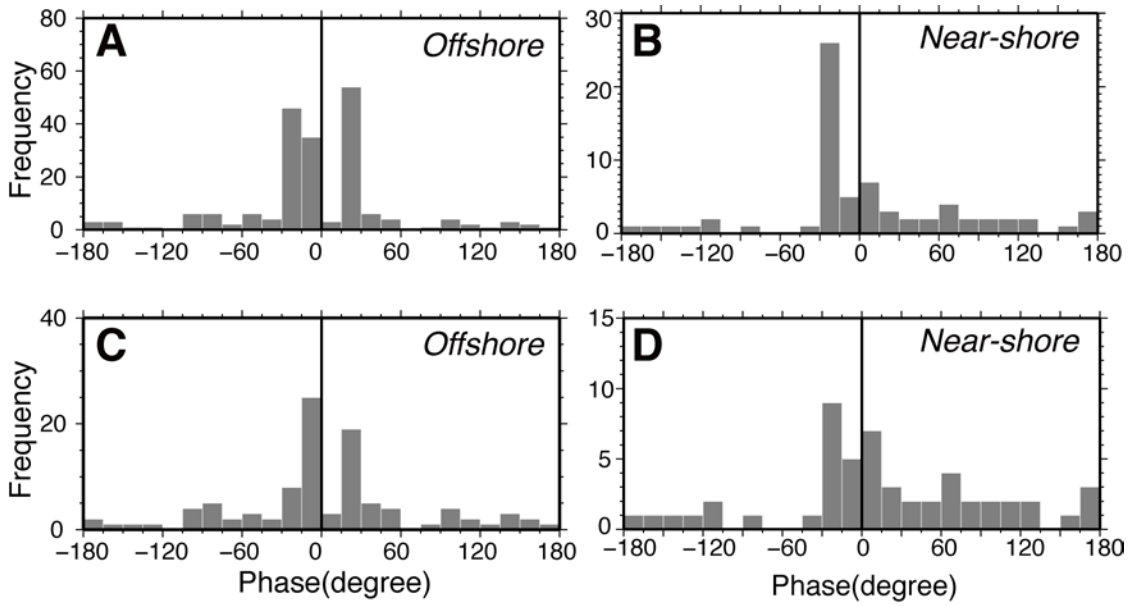

Fig. S7

Frequency distribution of M ≥ 5 earthquakes for each 15 degree bin of the phase of the sinusoidal curve fitted to repeater-derived slip rate for offshore and near-shore Sanriku, respectively. (A, B) original catalogue, (C, D) declustered catalogue by using Reasenberg's method. The phase zero is the peak of sinusoidal curve.

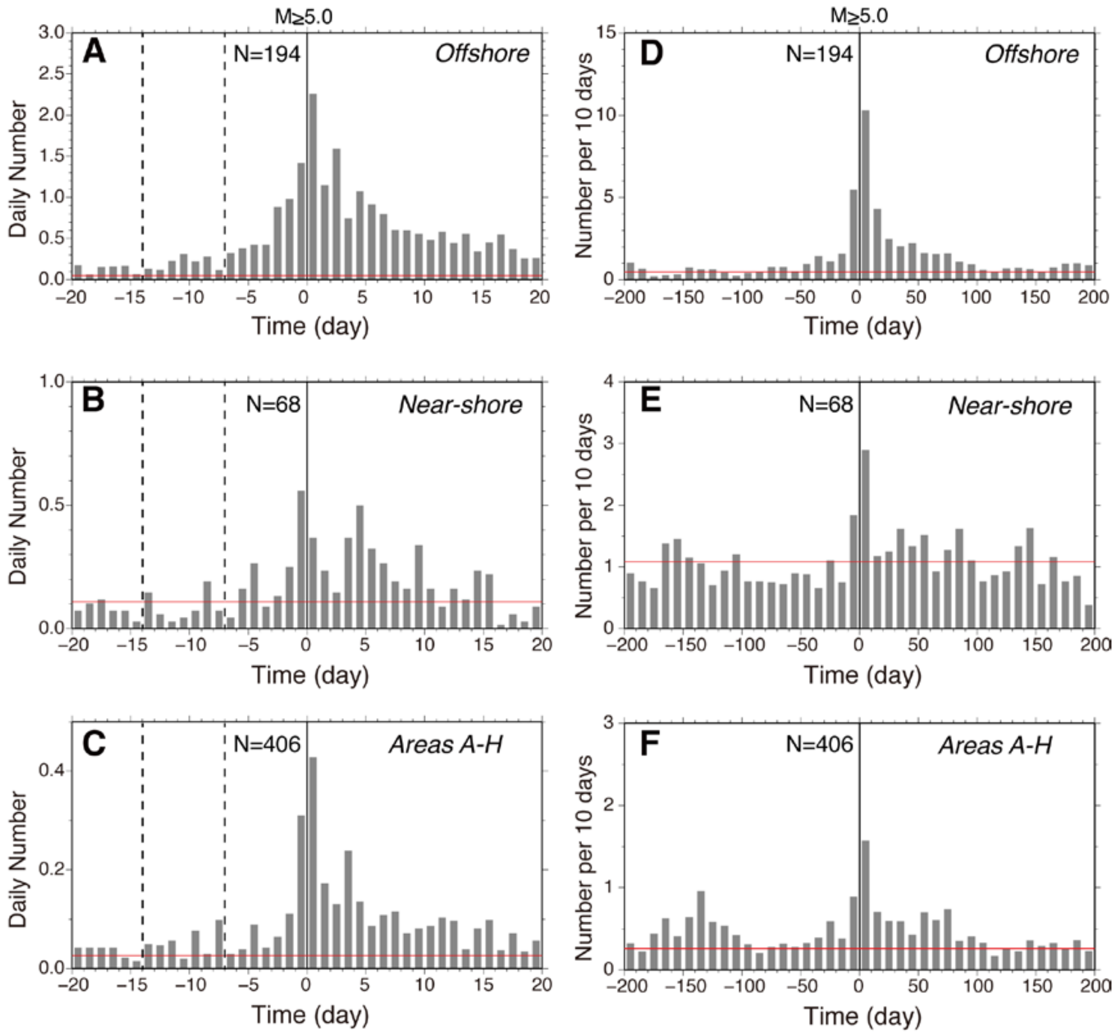

Fig. S8

Frequency distribution of repeating earthquakes before and after M≧5 mainshocks. The frequency is normalized by the number of mainshocks considered. (A-C) Daily number for offshore Sanriku, near-shore Sanriku and areas A-H shown in Fig. S2B. (D-F) The same but showing the number of repeaters per 10-day intervals over ± 200 days from the mainshocks. Vertical lines at zero denote the time of M≧5 earthquakes and the total number of mainshocks considered (*N*) is shown near the line. Vertical dashed lines mark three pre-mainshock periods for which spatial distribution of repeaters are shown in Figs S10 and S11. Horizontal red lines denote average daily (A-C) and 10 day (D-F) number of repeating earthquakes (normalized by *N*) in the whole analysis period.

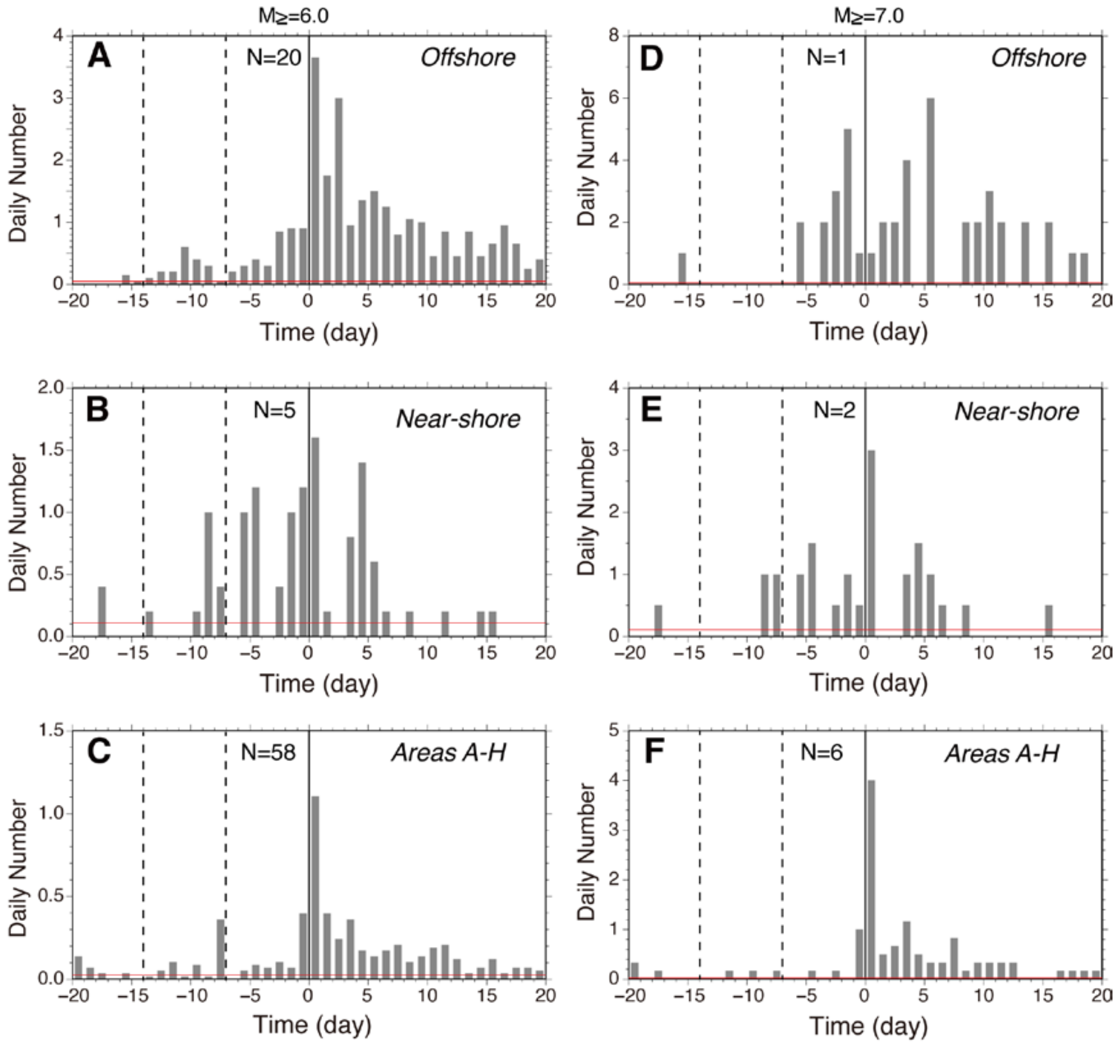

Fig. S9

Frequency distribution of repeating earthquakes before and after M≧6 (A-C) and M≧7 (D-F) mainshocks for offshore Sanriku, near-shore Sanriku and areas A-H. Daily numbers are shown. Other symbols are the same as Fig S8.

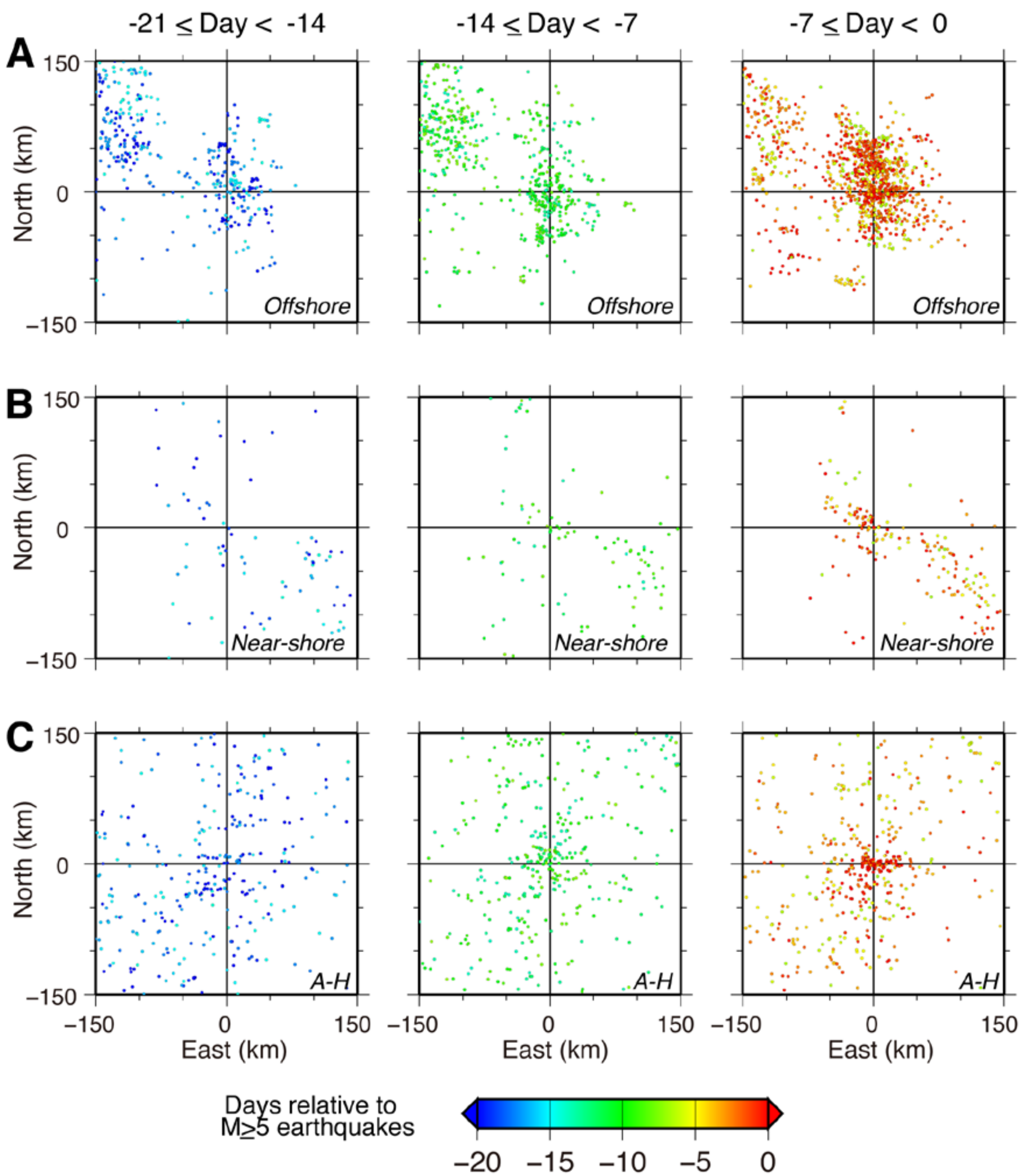

Fig. S10

Spatial distribution of repeating earthquakes relative to the epicenter of M ≧ 5 earthquakes in offshore Sanriku area (A), near-shore Sanriku area (B) and areas A-H (C) before the M≧5 earthquakes. Left, middle and right columns show the distribution in 21 to 14 days, 14 to 7 days and 7 to 0 days before the M≧5 mainshock earthquakes, respectively. The color of circles show the relative time to the M ≧ 5 mainshock earthquakes. The total number of mainshocks considered for each area are provided in Fig. S9.

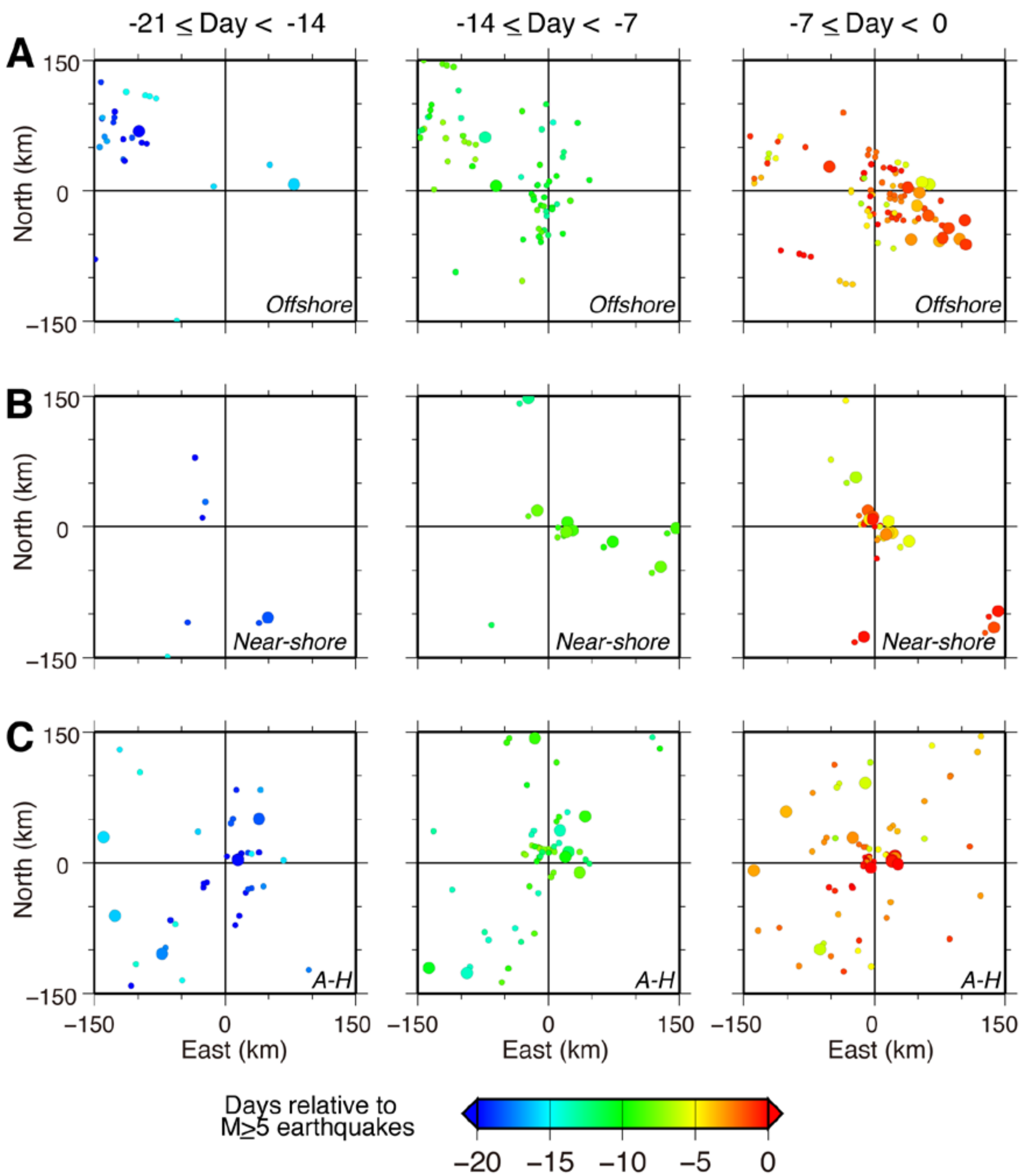

Fig. S11

Spatial distribution of repeating earthquake relative to the epicenter of M≧6 (small circles) and M≧7 (large circles) mainshock earthquakes in offshore Sanriku area (A) near-shore Sanriku area (B) and areas A-H (C). Left, middle and right columns show the distribution in 21 to 14 days, 14 to 7 days and 7 to 0 days before the mainshock earthquakes, respectively. The color of circles shows the relative time before mainshocks. The total number of mainshocks considered for each area are provided in Fig. S9.

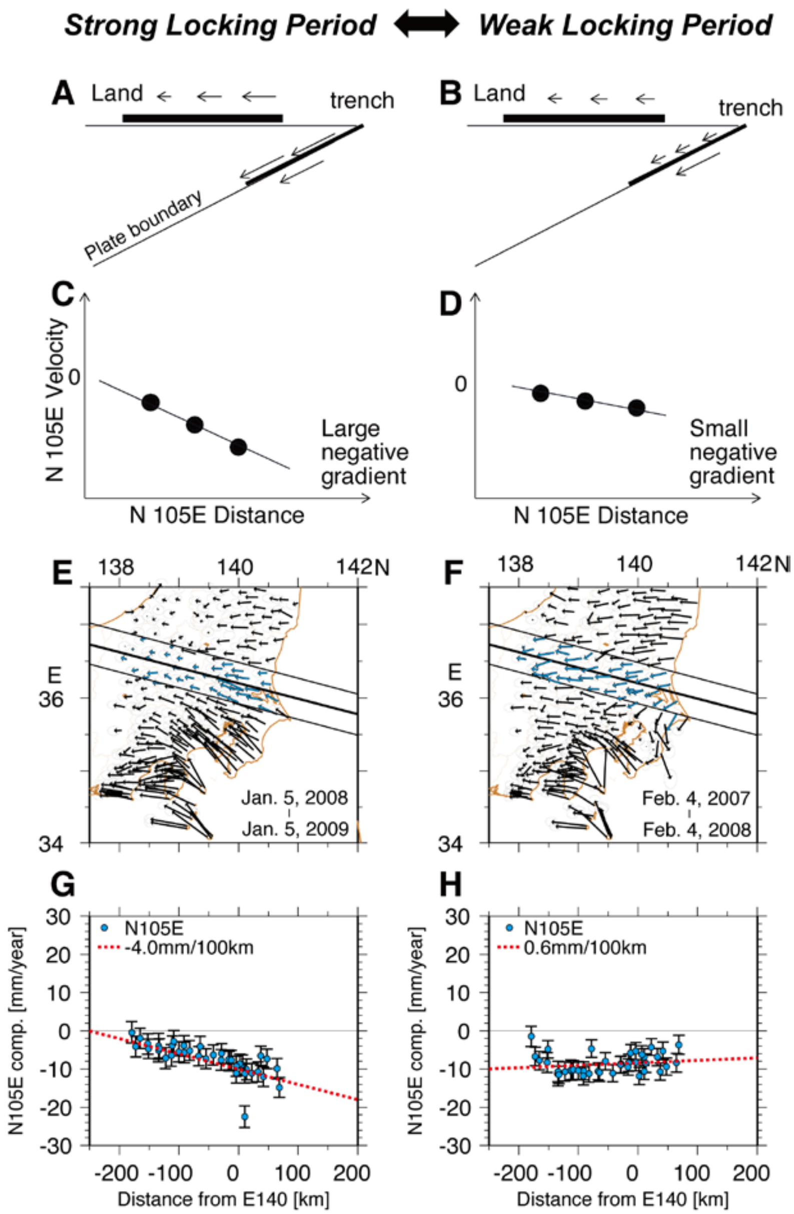

Fig. S12

Relationship between GPS-gradient and interplate locking. Left panels show strong locking period and right panels show weak locking period. (A) and (B) Schematic figures showing the interplate locking and surface deformation. (C) and (D) Schematic figures showing the relationship between distance along the subducting direction and horizontal ground velocity in subduction direction. (E) and (F) Examples of observed horizontal GPS velocity vectors offshore Ibaraki for the 1-year periods, starting from January 5, 2008 and February 4, 2007, respectively. (G) and (H) Examples of observed relationship between distance along the subducting direction (N105ºE) and horizontal ground velocity in the subduction direction for the periods shown in Figs (E) and (F), respectively. Each circle and error bars show velocity and its standard error, respectively.

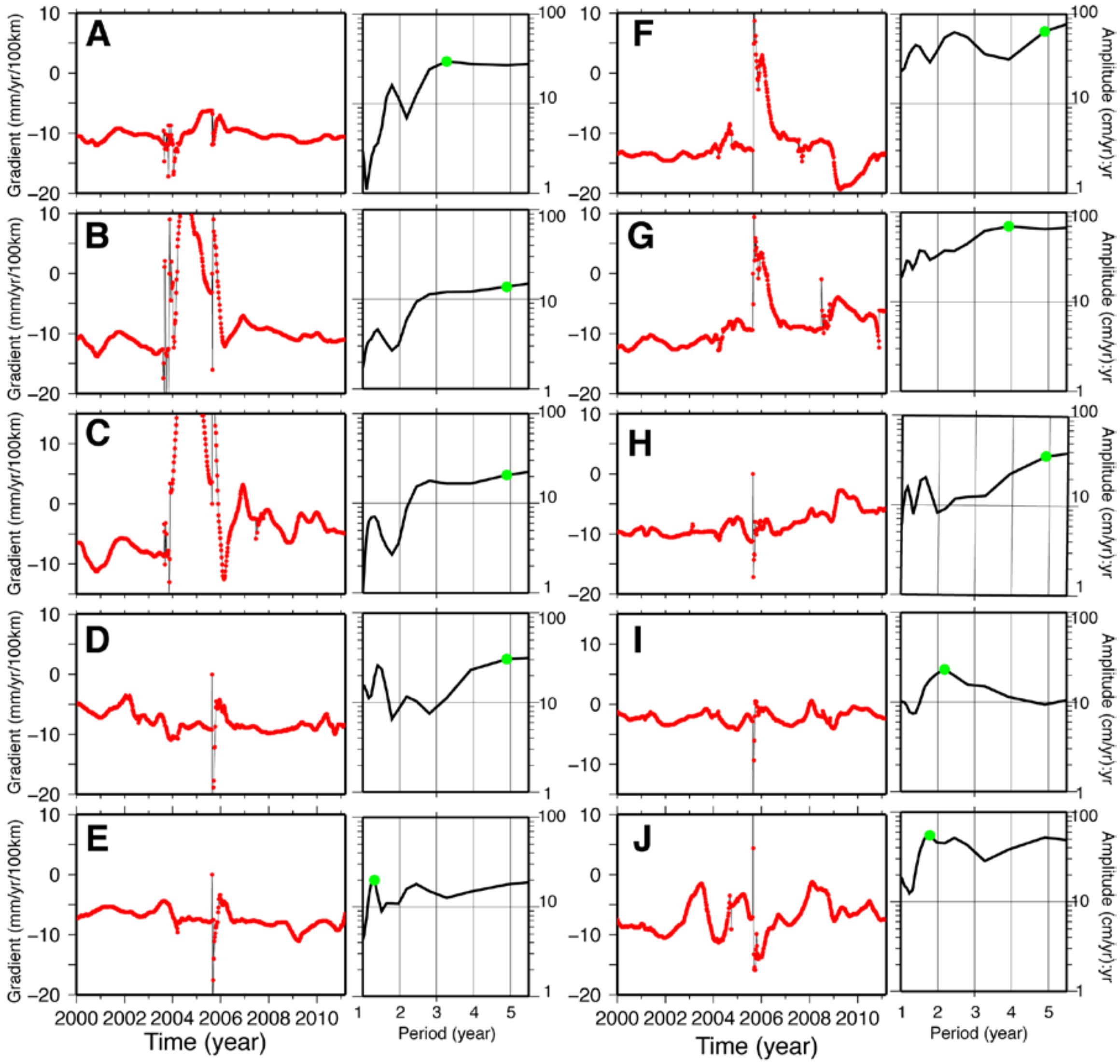

Fig. S13

Temporal change of the GPS velocity gradient and its spectra for profile lines a – j (A-J). The profile lines are shown in Fig. S2A. The disturbance around 2005 in a – j and around 2003-2004 in a – c are due to the M7.2 Miyagi-oki and M8.0 Tokachi-oki earthquake, respectively. Green dots in the right panels show the peak amplitude of the spectra.

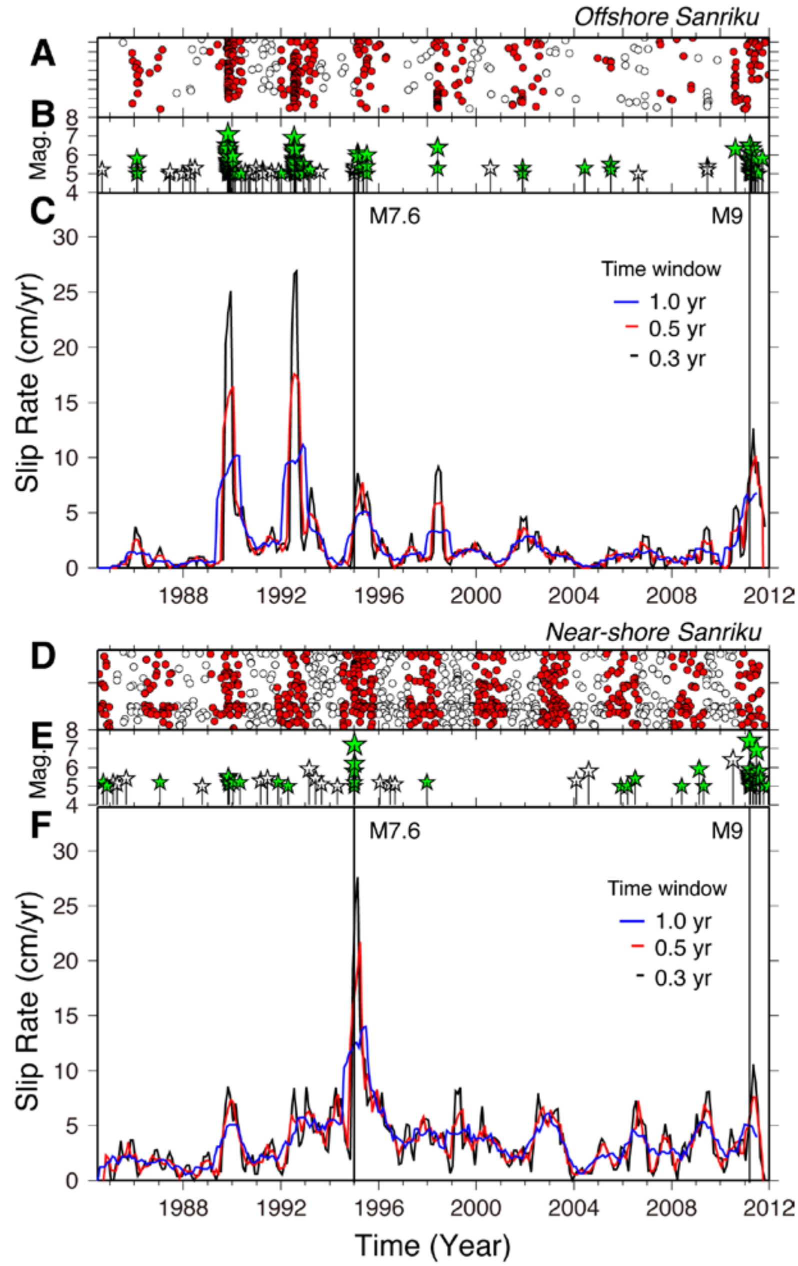

Fig. S14

Comparison of slip rate inferred from the analyses using different time-window lengths for offshore (A-C) and near-shore (D-F) Sanriku areas. Blue, red and black lines show slip rates from 1.0, 0.5 and 0.3 year time window analysis, respectively. Data are plotted at the center of each time window. Other panels are the same as Figs. 2B and C. The peak amplitudes depend on the time-window but the intervals between peaks and estimated periods do not change much.

Table S1 (separate file). The list of repeating earthquakes used in this study. The original data was reported by Uchida and Matsuzawa (2013) (*10*).

Table S2

Area	Period (year)	Uncertainty (year)	Number of Repeaters	N_{pos}/N_{neg} (Repeater)	Number of M≥=5 earthquakes	N_{pos}/N_{neg} (M≥5)	Probability [%] (M≥5) [1]
Offshore Sanriku	3.0	0.1	482	3.3	194	6.2	0.0
Near-shore Sanriku	2.7	0.6	1113	1.3	68	3.3	0.0
A	7.8	0.5	208	2.1	22	1.8	7.8
B	1.3	0.7	157	1.3	15	1.5	25
C	5.2	0.3	108	2.3	38	18	0.0
D	2.0	0.6	285	1.4	19	2.8	3.8
E	2.5	0.7	150	1.8	44	0.29	0.0
F	5.2	0.1	152	2.6	69	0.47	0.0
G	2.3	0.5	342	1.5	82	2.6	0.0
H	2.5	0.3	379	1.6	117	8.8	0.0

N_{pos} and N_{neg} mean number of earthquake in the positive and negative phase of sinusoid, respectively. For the N_{pos}/N_{neg} ratio, "inf" means the ratio is infinity (N_{neg} is zero) and "-" means the number of earthquake in the magnitude range is zero. Earthquakes in the depth range from 0 to 90km are used.

[1] Probability of earthquakes occurring in the positive period than the observed value to be by random chance.

[2] Earthquakes within 20 km from the plate models of Slab 1.0 (*42*) are used to count earthquake number.

Table S2 (Continue)

Area	Number of M≥=4 earthquakes	N_{pos}/N_{neg} (M≥4)	Probability [%] (M≥4) [1]	Number of M≥=6 earthquakes	N_{pos}/N_{neg} (M≥6)	Probability [%] (M≥6) [1]
Offshore Sanriku	413	6.8	0.0	18	inf	0.0
Near-shore Sanriku	189	2.9	0.0	6	5.0	10
A	51	2.9	0.0	4	inf	4.5
B	42	1.6	6.2	0	-	-
C	85	9.6	0.0	5	inf	3.1
D	46	1.9	2.7	2	inf	27
E	125	0.42	0.0	10	0.43	4.7
F	190	0.36	0.0	10	0.25	0.4
G	254	2.7	0.0	10	2.3	22
H	243	6.6	0.0	17	16	0.0

Table S2 (Continue)

Area	Number of M≥=5 earthquakes [2]	N_{pos}/N_{neg} (M≥5) [2]	Probability [%] (M≥5) [1, 2]
Offshore Sanriku	176	6.7	0.0
Near-shore Sanriku	69	3.3	0.0
A	15	2.8	2.9
B	14	1.3	34
C	37	36	0.0
D	18	2.6	5.5
E	33	0.32	0.0
F	38	0.58	2.0
G	68	2.6	0.0
H	59	11	0.0

Table S3 Ratio of the number of earthquakes in the positive and negative phases of the sinusoid (Npos/Nneg) as a function of the choice of declustering parameters for offshore Sanriku area. Numbers in parentheses are total number of $M \geq 5$ events in declustered catalogs. P and Q are related to the duration of interaction period and size of interaction zone, respectively.

	Q		
P	20	30	50
0.50	2.8 (79)	2.8 (76)	2.8 (76)
0.90	2.1 (64)	2.0 (59)	2.0 (59)
0.99	2.6 (75)	2.5 (69)	2.5 (69)

Table S4 The same as Table S3 for near-shore Sanriku area.

	Q		
P	20	30	50
0.50	1.2 (53)	1.2 (53)	1.2 (53)
0.90	1.2 (46)	1.2 (46)	1.2 (46)
0.99	1.2 (53)	1.2 (53)	1.2 (53)

REFERENCES AND NOTES

1. K. Heki, S. Miyazaki, H. Tsuji, Silent fault slip following an interplate thrust earthquake at the Japan Trench. *Nature* **386**, 595–598 (1997). doi:10.1038/386595a0

2. G. Dragert, K. Wang, T. S. James, A silent slip event on the deeper Cascadia subduction interface. *Science* **292**, 1525–1528 (2001). Medline doi:10.1126/science.1060152

3. P. Segall, A. M. Bradley, Slow-slip evolves into megathrust earthquakes in 2D numerical simulations. *Geophys. Res. Lett.* **39**, L18308 (2012). doi:10.1029/2012GL052811

4. A. Kato, K. Obara, T. Igarashi, H. Tsuruoka, S. Nakagawa, N. Hirata, Propagation of slow slip leading up to the 2011 M_w 9.0 Tohoku-Oki earthquake. *Science* **335**, 705–708 (2012). Medline doi:10.1126/science.1215141

5. M. Bouchon, V. Durand, D. Marsan, H. Karabulut, J. Schmittbuhl, The long precursory phase of most large interplate earthquakes. *Nat. Geosci.* **6**, 299–302 (2013. doi:10.1038/ngeo1770

6. S. Ruiz, M. Metois, A. Fuenzalida, J. Ruiz, F. Leyton, R. Grandin, C. Vigny, R. Madariaga, J. Campos, Intense foreshocks and a slow slip event preceded the 2014 Iquique Mw 8.1 earthquake. *Science* **345**, 1165–1169 (2014). Medline doi:10.1126/science.1256074

7. S. Ozawa, H. Suito, M. Tobita, Occurrence of quasi-periodic slow-slip off the east coast of the Boso peninsula, Central Japan. *Earth Planets Space* **59**, 1241–1245 (2007). doi:10.1186/BF03352072

8. R. M. Nadeau, T. V. McEvilly, Fault slip rates at depth from recurrence intervals of repeating microearthquakes. *Science* **285**, 718–721 (1999). 10.1126/science.285.5428.718 Medline doi:10.1126/science.285.5428.718

9. R. M. Nadeau, T. V. McEvilly, Periodic pulsing of characteristic microearthquakes on the San Andreas fault. *Science* **303**, 220–222 (2004). Medline doi:10.1126/science.1090353

10. N. Uchida, T. Matsuzawa, Pre- and postseismic slow slip surrounding the 2011 Tohoku-oki earthquake rupture. *Earth Planet. Sci. Lett.* **374**, 81–91 (2013). doi:10.1016/j.epsl.2013.05.021

11. Y. Yamanaka, M. Kikuchi, Source process of the recurrent Tokachi-oki earthquake on September 26, 2003, inferred from teleseismic body waves. *Earth Planets Space* **55**, e21–e24 (2003). doi:10.1186/BF03352479

12. Y. Yamanaka, M. Kikuchi, Asperity map along the subduction zone in northeastern Japan inferred from regional seismic data. *J. Geophys. Res.* **109**, B07307 (2004). doi:10.1029/2003JB002683

13. T. Iinuma, R. Hino, M. Kido, D. Inazu, Y. Osada, Y. Ito, M. Ohzono, H. Tsushima, S. Suzuki, H. Fujimoto, S. Miura, Coseismic slip distribution of the 2011 off the

Pacific Coast of Tohoku Earthquake (M9.0) refined by means of seafloor geodetic data. *J. Geophys. Res.* **117**, B07409 (2012). doi:10.1029/2012JB009186

14. Materials and methods are available as supplementary materials on *Science* Online
15. G. F. Sella, T. H. Dixon, A. Mao, REVEL: A model for Recent plate velocities from space geodesy. *J. Geophys. Res.* **107**, 2081 (2002). doi:10.1029/2000JB000033
16. N. Uchida, A. Hasegawa, T. Matsuzawa, T. Igarashi, Pre- and post-seismic slip on the plate boundary off Sanriku, NE Japan associated with three interplate earthquakes as estimated from small repeating earthquake data. *Tectonophysics* **385**, 1–15 (2004). doi:10.1016/j.tecto.2004.04.015
17. D. Marsan, T. Reverso, A. Helmstetter, B. Enescu, Slow slip and aseismic deformation episodes associated with the subducting Pacific plate offshore Japan, revealed by changes in seismicity. *J. Geophys. Res. Solid Earth* **118**, 4900–4909 (2013). 10.1002/jgrb.50323 doi:10.1002/jgrb.50323
18. Y. Ito, R. Hino, M. Kido, H. Fujimoto, Y. Osada, D. Inazu, Y. Ohta, T. Iinuma, M. Ohzono, S. Miura, M. Mishina, K. Suzuki, T. Tsuji, J. Ashi, Episodic slow slip events in the Japan subduction zone before the 2011 Tohoku-Oki earthquake. *Tectonophysics* **600**, 14–26 (2013). doi:10.1016/j.tecto.2012.08.022
19. T. J. Ader, J.-P. Avouac, Detecting periodicities and declustering in earthquake catalogs using the Schuster spectrum, application to Himalayan seismicity. *Earth Planet. Sci. Lett.* **377-378**, 97–105 (2013).
20. J. C. Savage, A dislocation model of strain accumulation and release at a subduction zone. *J. Geophys. Res. Solid Earth* **88**, 4984–4996 (1983). doi:10.1029/JB088iB06p04984
21. K. Heki, Snow load and seasonal variation of earthquake occurrence in Japan. *Earth Planet. Sci. Lett.* **207**, 159–164 (2003). doi:10.1016/S0012-821X(02)01148-2
22. Y. Tanaka, An approximately 9-yr-period variation in seismicity and crustal deformation near the Japan Trench and a consideration of its origin. *Geophys. J. Int.* **196**, 760–787 (2014). doi:10.1093/gji/ggt424
23. F. F. Pollitz, A. Wech, H. Kao, R. Bürgmann, Annual modulation of non-volcanic tremor in northern Cascadia. *J. Geophys. Res. Solid Earth* **118**, 2445–2459 (2013). 10.1002/jgrb.50181 doi:10.1002/jgrb.50181
24. Y. Liu, Numerical simulations on megathrust rupture stabilized under strong dilatancy strengthening in slow slip region. *Geophys. Res. Lett.* **40**, 1311–1316 (2013). 10.1002/grl.50298 doi:10.1002/grl.50298
25. P. Segall, A. M. Rubin, A. M. Bradley, J. R. Rice, Dilatant strengthening as a mechanism for slow slip events. *J. Geophys. Res. Solid Earth* **115**, B12305 (2010). 10.1029/2010JB007449 doi:10.1029/2010JB007449
26. P. Audet, R. Bürgmann, Possible control of subduction zone slow-earthquake periodicity by silica enrichment. *Nature* **510**, 389–392 (2014).

27. R. Hino, D. Inazu, Y. Ohta, Y. Ito, S. Suzuki, T. Iinuma, Y. Osada, M. Kido, H. Fujimoto, Y. Kaneda, Was the 2011 Tohoku-Oki earthquake preceded by aseismic preslip? Examination of seafloor vertical deformation data near the epicenter. *Mar. Geophys. Res.* **35**, 181–190 (2014). doi:10.1007/s11001-013-9208-2

28. S. Ozawa, T. Nishimura, H. Munekane, H. Suito, T. Kobayashi, M. Tobita, T. Imakiire, Preceding, coseismic, and postseismic slips of the 2011 Tohoku earthquake, Japan. *J. Geophys. Res.* **117**, B07404 (2012). 10.1029/2011JB009120 doi:10.1029/2011JB009120

29. T. H. Jordan, L. M. Jones, Operational earthquake forecasting: Some thoughts on why and how. *Seismol. Res. Lett.* **81**, 571–574 (2010). doi:10.1785/gssrl.81.4.571

30. T. Murotani, M. Kikuchi, Y. Yamanaka, "Rupture processes of large Fukushima-Oki earthquakes in 1938," paper S052-004, presented at the 2003 Japan Geoscience Union, Chiba, Japan, 2003.

31. N. Uchida, T. Matsuzawa, W. L. Ellsworth, K. Imanishi, K. Shimamura, A. Hasegawa, Source parameters of microearthquakes on an interplate asperity off Kamaishi, NE Japan over two earthquake cycles. *Geophys. J. Int.* **189**, 999–1014 (2012). 10.1111/j.1365-246X.2012.05377.x doi:10.1111/j.1365-246X.2012.05377.x

32. R. M. Nadeau, L. R. Johnson, Seismological studies at Parkfield VI: Moment release rates and estimates of source parameters for small repeating earthquakes. *Bull. Seismol. Soc. Am.* **88**, 790–814 (1998).

33. T. C. Hanks, H. Kanamori, A moment magnitude scale. *J. Geophys. Res.* **84**, 2348–2350 (1979). 10.1029/JB084iB05p02348 doi:10.1029/JB084iB05p02348

34. K. H. Chen, R. M. Nadeau, R. J. Rau, Towards a universal rule on the recurrence interval scaling of repeating earthquakes? *Geophys. Res. Lett.* **34**, L16308 (2007). doi:10.1029/2007GL030554

35. C. Goltz, D. L. Turcotte, S. G. Abaimov, R. M. Nadeau, N. Uchida, T. Matsuzawa, Rescaled earthquake recurrence time statistics: Application to microrepeaters. *Geophys. J. Int.* **176**, 256–264 (2009). doi:10.1111/j.1365-246X.2008.03999.x

36. T. Igarashi, T. Matsuzawa, A. Hasegawa, Repeating earthquakes and interplate aseismic slip in the northeastern Japan subduction zone. *J. Geophys. Res.* **108**, 2249 (2003). 10.1029/2002JB001920 doi:10.1029/2002JB001920

37. A. P. Mavrommatis, P. Segall, N. Uchida, K. M. Johnson, Long-term acceleration of aseismic slip preceding the Mw 9 Tohoku-oki earthquake: Constraints from repeating earthquakes. *Geophys. Res. Lett.* 2015GL066069 (2015).

38. N. M. Beeler, D. L. Lockner, S. H. Hickman, A simple stick-slip and creep-slip model for repeating earthquakes and its implication for microearthquakes at Parkfield. *Bull. Seismol. Soc. Am.* **91**, 1797–1804 (2001). doi:10.1785/0120000096

39. Y. Suwa, S. Miura, A. Hasegawa, T. Sato, K. Tachibana, Interplate coupling beneath NE Japan inferred from three dimensional displacement field. *J. Geophys. Res.* **111**, 101029/102004JB003203 (2006).

40. A. P. Mavrommatis, P. Segall, K. M. Johnson, A decadal-scale deformation transient prior to the 2011 M_w 9.0 Tohoku-oki earthquake. *Geophys. Res. Lett.* **41**, 4486–4494 (2014). 10.1002/2014gl060139

41. P. Reasenberg, Second-order moment of central California seismicity, 1969–1982. *J. Geophys. Res. Solid Earth* **90**, 5479–5495 (1985). doi:10.1029/JB090iB07p05479

42. G. P. Hayes, D. J. Wald, R. L. Johnson, Slab1.0: A three-dimensional model of global subduction zone geometries. *J. Geophys. Res. Solid Earth* **117**, B01302 (2012). 10.1029/2011JB008524